Northumbria Research Link

Exploring the Differences between Forward Osmosis and Reverse Osmosis Fouling

Farrukh Arsalan Siddiqui [a,1], Qianhong She [b,c*], Anthony G. Fane [b,d], Robert W. Field [a**]

[a] Department of Engineering Science, University of Oxford, United Kingdom
[b] Singapore Membrane Technology Centre, Nanyang Environment & Water Research Institute, Nanyang Technological University, Singapore
[c] School of Chemical and Biomolecular Engineering, The University of Sydney, NSW 2006, Australia
[d] UNESCO Centre for Membrane Science and Technology, University of New South Wales, NSW 2052, Australia

[*] Corresponding author address: The University of Sydney, Room 494, Level 4, Chemical Engineering Building J01, Darlington, NSW 2006, Australia; Tel: +61 2 8627 6071; Fax: +61 2 9351 2854; Email: qianhong.she@sydney.edu.au

[**] Corresponding author address: University of Oxford, Parks Road, Oxford, OX1 3PJ, UK; Tel: +44 1865 273181; Fax: +44 1865 273010; Email: robert.field@eng.ox.ac.uk

[1] Permanent address: Department of Mechanical Engineering, Bahauddin Zakariya University, Bosan Road, Multan 60800, Pakistan

38 **Abstract**

39 A comparison of alginate fouling in forward osmosis (FO) with that in reverse osmosis (RO)

40 was made. A key experimental finding, corroborated by membrane autopsies, was that FO is

41 essentially more prone to fouling than RO, which is opposite to a common claim in the

42 literature where deductions on fouling are often based solely on the water flux profiles. Our

43 theoretical analysis shows that, due to a decrease in the intensity of internal concentration

44 polarization (ICP), and thus an increase in the effective osmotic driving force during FO fouling

45 tests, the similarity of experimental water flux profiles for FO and RO is in accordance with

46 there being greater fouling in FO than RO. The specific foulant resistance for FO was also

47 found to be greater than that for RO. Possible explanations are discussed and these include the

48 influence of reverse solute diffusion from draw solution. Whilst this explanation regarding

49 specific foulant resistance is dependent on the draw solution properties, the finding of greater

50 overall foulant accumulation in FO is considered to be a general finding. Additionally, the

51 present study did not find evidence that hydraulic pressure in RO plays a critical role in foulant

52 layer compaction. Overall this study demonstrated that although FO has higher fouling

53 propensity, it offers superior water flux stability against fouling. For certain practical

54 applications this resilience may be important.

55

56

57 **Keywords**: forward osmosis; reverse osmosis; fouling; internal concentration polarization

58 (ICP); cake-enhanced concentration polarization (CECP)

59

60

61 **Graphic Abstract**

62

A

- Fouling	→	- Reduce J_w	→	- ICP Self-compensation	→	- Increase effective	→	- Partial flux compensation	→	- More foulant deposition	→	FO fouling
- Increase R_f				- Reduce ICP		driving force		- Compensate J_w decline		- Greater drag compaction		evolves
				- Increase $\pi_{ds,i}$		($\Delta\pi_{eff} = \pi_{ds,i} - \pi_{fs,m}$)				- Greater increase of R_f		

- Cake-enhanced
concentration polarization
- Increase $\pi_{fs,m}$

B

- Fouling	→	- Reduce J_w	→	- Decrease effective	→	- Less foulant deposition	→	RO fouling
- Increase R_f				driving force ($\Delta P - \Delta\pi$)		- Lower drag compaction		evolves
						- Smaller increase of R_f		

- Cake-enhanced
concentration polarization
- Increase $\pi_{fs,m}$

63
64
65
66

3

1. Introduction

Forward osmosis (FO) has received considerable interest in the recent decade for various applications such as desalination [1-4], wastewater treatment [3-6], trace contaminant removal [7-9], and resource recovery [10, 11]. In an FO process a draw solution (DS) with a higher osmotic pressure on one side of a selective membrane draws the water from a feed solution (FS) with a lower osmotic pressure on the other side of the membrane [1]. Unlike pressure-driven reverse osmosis (RO) that is a relatively energy-intensive process, osmotically driven FO process only requires minimum electrical energy for pumping the DS and FS solutions. In those special cases where the application does not require the regeneration of the DS (e.g., the osmotic dilution of the fertilizer-based DS [12] and/or the concentration of the FS for nutrient recovery [10]), FO has an outstanding advantage in terms of lower energy consumption. Also it has been suggested that a hybrid FO system that incorporates a DS regeneration process may also outperform conventional RO when treating challenging feedwaters (e.g., the feedwater with high salinity or specific challenging contaminants) [4, 13, 14]. Whilst energy consumption is a major factor in the evaluation between FO and RO [13, 15, 16], membrane fouling is another important consideration when comparing the performance of FO and RO in practical applications [3-5, 13, 14, 17].

1.1. Critical review of prior studies on the comparison of fouling in FO and RO

Owing to the different driving forces for FO and RO (i.e., osmotic pressure vs. hydraulic pressure), fouling behaviour between FO and RO has been presumed to be different. The comparison of membrane fouling between FO and RO processes has been studied extensively and it has been broadly claimed that osmotically driven FO has lower fouling tendency and greater fouling reversibility than pressure-driven RO [13, 18-28]. These studies attributed their claim to the lack of hydraulic compaction of the foulant layer in the FO process, which resulted

4

92   in the formation of different foulant layer structure in FO compared to that in RO. They stated

93   that in FO the foulant layer is looser and less compacted and thereby the fouled membrane can

94   be easily cleaned by a brief water rinsing, whereas in RO the foulant layer is densely compacted

95   and tightly held on the membrane under the action of hydraulic pressure, thereby resulting in a

96   reduced cleaning efficiency [19, 24].

97

98   On the other hand, a number of other studies have reported opposing observations [29-32]. Lay

99   et al. did not observe differences in the flux decline between FO and RO fouling and they

100 attributed this to the low initial water flux that was said to be below the critical flux [29], which

101 today might be better termed threshold flux [33]. For alginate and silica fouling, Jang et al.

102 observed in a laboratory study that fouling propensity was the highest for FO compared with

103 RO and membrane distillation [30]. Tow et al. developed a method of *in situ* membrane fouling

104 quantification and found greater foulant accumulation with FO than with RO, which suggests

105 that fouling in FO might be more severe than RO despite the observed lower flux decline in

106 FO [31]. In addition, their study did not find any evidence that the thinner cake layer (less

107 foulant accumulation) in RO could be attributed to the hydraulic pressure compaction [31]. In

108 an earlier study on alginate and silica fouling in RO under constant flux operation, Fane and

109 Chong observed no clear difference in the trans-membrane pressure (TMP) profiles for a flux

110 of 40 l/m^{2}hr (well above the critical flux for both foulants) with varying feed pressures from

111 22 to 30 bar, suggesting that foulant layer compaction is physically related to water flux not

112 hydraulic pressure *per se* [32].

113

114 **1.2. Analysis of possible reasons for the different findings on FO and RO fouling**

115 The inconsistent findings on FO and RO fouling between different groups of researchers

116 probably lie in the discrepancies with respect to experimental methods used, as well as in the

different analytical approaches. Firstly, in most of the prior studies experimental conditions for FO and RO were not comparably controlled. For example, (i) in many cases the apparent driving force for RO (i.e., hydraulic pressure, ΔP) was maintained constant during the entire RO experimental test, whereas that for FO (i.e., osmotic pressure difference between the bulk DS and the bulk FS, $\Delta \pi$) was gradually decreasing during the FO experimental test as the DS was gradually diluted and the FS was gradually concentrated [19-21, 23, 24, 30, 31, 34]; (ii) different types of membranes were used for FO and RO tests, for which different membrane properties may influence the fouling behaviour [26, 31]. Secondly, in many prior studies the reported water flux for RO was directly observed from experiments, whereas for FO it was not the experimentally observed flux but a corrected one by using experimental fouling flux and baseline flux under non-fouling conditions [19-24]. Typically, the approach to correct the observed FO flux was to eliminate the effects of DS dilution and the FS concentration during the test. However, the approach of flux correction did not take into account the effects of concentration polarization (CP) especially internal concentration polarization (ICP) that is strongly dependent on the solution concentration and will significantly influence the observed flux via the change in effective driving force [35-37]. Thirdly, the majority of prior studies compared the fouling propensity between FO and RO based on the extent of flux decline [19-24, 26, 30, 34]. However, in both FO and RO, especially FO, temporal changes in flux do not properly reflect the evolution of foulant accumulation on the membrane, because the flux decline is related not only to the hydraulic resistance of the foulant layer accumulated on the membrane but also to the CP that will result in the decrease of effective driving force [20, 31, 36-39]. It is also noted that the foulant layer formed on the membrane might influence the degree of external CP through the process of "cake-enhanced concentration polarization" [38]. Although Tow et al. developed a method to quantify membrane fouling by employing two parameters – cake structural parameter (that is related to cake-enhanced concentration

142   polarization) and pore hydraulic diameter (that is related to hydraulic resistance of foulant

143   layer), it appears that their study only focused on the analysis of the former under conditions

144   where cake hydraulic resistance is negligible [31].

145

146   **1.3. Definition of fouling and objectives of the current study**

147   The controversy over FO and RO fouling in prior studies has provided an impetus for us to

148   perform an insightful comparison of fouling between FO and RO processes. It is noted that the

149   majority of prior studies comparing fouling between FO and RO were based solely on the water

150   flux profiles [18-26]. It was generally assumed that a water decline was an appropriate metric

151   for fouling behaviour in both cases [18-26]. However, this overlooks a key difference between

152   fouling in FO compared with that in RO. This is because water flux decline is dependent not

153   only on fouling but also on driving force (i.e., osmotic pressure for FO and hydraulic pressure

154   for RO), as shown below:

155    $J = \frac{F}{\mu R}$ (1)

156   where J is water flux, F is driving force, μ is viscosity of the solution, and R is the overall

157   hydraulic resistance of membrane and foulant layer.

158   Now in this study we specifically define that *fouling* is the accumulation of foulant on the

159   membrane, and is quantified by the foulant layer resistance (R_f), which is consistent with

160   previous studies quantifying fouling of desalination membranes [32, 40-42]. As CP is flux

161   dependent, fouling will change the effective driving forces in FO and RO because of changes

162   in CP. Due to ICP changing with water flux, the changes in effective driving force are

163   particularly significant for FO [36, 37]. Therefore, for FO processes, an examination of the

164   decline in flux in isolation does not properly reflect the extent of fouling (i.e., the evolution of

165   foulant accumulation on the membrane).

166

7

167   Consequently the current study aims to compare the fouling between FO and RO focusing on

168   the comparison of hydraulic resistances of the foulant layers with due allowance for the CP

169   effects. A specific objective is to have a mechanistic understanding of the differences of fouling

170   and its influences on water flux between FO and RO. To enable a fair comparison our

171   experiments were designed to use the same membranes, have essentially the same initial water

172   flux, and have well controlled conditions including constant overall driving force, throughout

173   the complete experiments as detailed in section 2.2.

174

175   **2. Materials and Methods**

176   **2.1. Chemicals and membranes**

177   Unless otherwise stated, all the chemicals used in this study were of analytical grade. Ultrapure

178   deionised (DI) water which was supplied by a Milli-Q Ultrapure water system (Millipore

179   Singapore Pte Ltd) with a resistivity of 18.2 MΩ cm was used to prepare all the solutions.

180   Sodium salt of alginic acid (alginate, Sigma-Aldrich St. Louis, MO) was used as model foulant

181   to study membrane fouling. It gives gel-layer fouling rather than cake-layer fouling but the

182   term cake-enhanced concentration polarization (CECP) has been retained in this paper. The

183   feed solution in both FO and RO fouling experiments was composed of 45 mM NaCl, 5 mM

184   CaCl$_2$ and 200 mg/L alginate. The draw solution for FO experiments was composed of 1.5 M

185   NaCl. The initial volume of the feed solution and draw solution was 5 L.

186

187   A cellulose triacetate (CTA) membrane provided by Hydration Technology Innovations (HTI,

188   Albany, OR) was used in both FO and RO experimental tests. The CTA membrane comprised

189   a dense selective layer and a porous support layer embedded within a polyester woven mesh

190   fabric. This membrane has been widely used as a model membrane to compare fouling in FO

191   and RO [19-21, 31]. The reason for the use of the same membrane in both FO and RO tests is

8

192   to eliminate the influence of membrane materials on fouling and thus generate a fair

193   comparison between fouling in FO and RO.

194

195   **2.2. FO and RO membrane fouling experiments**

196   The same experimental setup was used for FO and RO experimental tests with only slight

197   modification between the two different test modes (Fig. S1 in Supporting Information S1). This

198   setup has also been used in our previous osmotic membrane fouling experiments and benefits,

199   *inter alia*, from being able to maintain a constant draw concentration [43]. The setup had a PLC

200   control system that allowed automatic control of experimental operation and data acquisition.

201   For FO tests, both FS and DS were recirculated with Hydra-Cell positive displacement

202   diaphragm pumps (Fig. S1A). The FO membrane test cell (CF042, Sterlitech Corporation) was

203   comprised of two symmetric Delrin half-cells (top cell and bottom cell) with identical

204   dimension of flow channel (85 mm length $\times$ 39 mm width $\times$ 2.3 mm height). A net spacer was

205   placed in the DS flow channel to enhance the mixing and mass transfer of DS [44]. The DS

206   cross-flow velocity was 11.1 cm/s. The draw solution conductivity (and thus concentration)

207   was maintained constant by dosing with a more concentrated NaCl solution. The feed solution

208   conductivity was monitored with time to estimate the reverse solute flux following the same

209   methods described previously [44]. For RO tests, only FS was recirculated, while the permeate

210   water was collected directly in a permeate tank (Fig. S1B). There was dosing of the feed with

211   DI water to ensure concentration was kept constant. The RO membrane test cell had the same

212   FS flow channel as that for FO. The permeate channel was filled with sintered porous metal

213   plate (with ~20 μm mean pore size) that could fully support the membrane against deformation

214   in the RO test. The feed and permeate conductivity were monitored with time to estimate the

215   rejection.

216

217   For both FO and RO tests, the FS tank was placed on a digital balance and the FS mass (and

218   thus FS volume and foulant concentration) was maintained constant via continuous dosing with

219   DI water (see Fig S1B). Small amounts of salt leakage did occur from the DS side but the

220   increase in bulk FS concentration was marginal due to large volume (5 L) of FS used in the

221   experiments and its influence on the bulk DS and FS osmotic pressure difference is negligible

222   according to conductivity monitoring. The mass change of the DI water with time was recorded

223   and used to determine the water flux. No feed spacer was placed in the FS channel to accelerate

224   fouling. The membrane active layer was facing the FS. The cross-flow velocity of FS was 7.4

225   cm/s. The apparent driving forces for both RO and FO (i.e., the applied hydraulic pressure for

226   RO and the osmotic pressure difference between the bulk DS and the bulk FS for FO) were

227   maintained constant.

228

229   After each fouling test, the fouled membrane was either cleaned via surface flushing to

230   investigate the fouling reversibility or autopsied to determine the foulant deposition. During

231   surface flushing, the FS was replaced with DI water and the cross-flow velocity of FS was

232   increased to 29.6 cm/s. For the FO fouled membrane the DS was also replaced with DI and not

233   recirculated; for the RO fouled membrane the applied hydraulic pressure was reduced to zero.

234   In both cases the surface flushing was performed for 30 minutes. The foulant mass load (i.e.,

235   amount of foulant deposited on unit area of membrane surface) was determined by foulant

236   extraction followed by measurement of the total organic carbon (TOC) using a similar protocol

237   reported elsewhere [43]. The protocol is briefly summarized in Supporting Information S2.

238

239   **2.3. Determination of foulant resistance for fouled membranes in FO and RO**

240   Before the determination of the foulant resistance on the fouled membranes (R_f), the clean

241   membrane resistance (R_m) was first measured via a RO test using a foulant-free feed solution

242   with the same background electrolyte used for the fouling test. The R_m for the clean membrane

243   was estimated using the following osmotic-resistance filtration (ORF) model for RO that was

244   reported elsewhere [45] and can be simplified from the universal ORF model for osmotically

245   driven membrane processes (ODMPs) ([37] and Appendix A).

246    $$J_w = \frac{\Delta P - \eta_{rej}\pi_{fs} exp\left(\frac{J_w}{k_{ecp}}\right)}{\mu R_m} \tag{2}$$

247   where ΔP is the effective applied hydraulic pressure, η_{rej} is the solute rejection that was

248   determined based on conductivity measurement of permeate and feed water, π_{fs} is the osmotic

249   pressure of the feed solution (that can be correlated by the van't Hoff equation $\pi = C\beta R_g T$

250   where C is concentration, β is van't Hoff coefficient, R_g is the universal gas constant and T is

251   temperature), J_w is the water flux, k_{cecp} is the mass transfer coefficient near the membrane

252   surface, and μ is the viscosity of the feed solution. The membrane resistance R_m is related to

253   the water permeability coefficient (A) by $A = 1/\mu R_m$. Note that external concentration

254   polarization (ECP) has been incorporated in Eq. (2) and that for the feed channel k_{ecp} can be

255   estimated following the approach reported elsewhere [46].

256

257   The structural parameter (S) of the FO membrane was determined by inputting π_{ds} and π_{fs},

258   and the foulant-free experimentally obtained parameters (i.e., J_w, J_s/J_w, R_m) into the following

259   equation that is rearranged from the ORF model [37].

260    $$S = \frac{D}{J_w} \ln\left[\frac{\pi_{ds}+\frac{J_s}{J_w}\beta R_g T}{\left(\pi_{fs}+\frac{J_s}{J_w}\beta R_g T\right)exp\left(\frac{J_w}{k_{ecp}}\right)+\mu R_m J_w}\right] \tag{3}$$

261   The value of k_{ecp} was the same value as that estimated for RO because the membrane cell for

262   the FO tests and RO tests had the same feed-side flow channel hydrodynamics.

263

264   The foulant resistance (R_f) on the RO fouled membrane was determined by inputting π_{fs}, ΔP,

265   and the experimentally obtained $J_{w,f}$, $\eta_{rej,f}$ into Eq. (4) which, through the term $k_{ecp,f}$,

266   includes an adjustment for cake-enhanced concentration polarization (CECP).

267    $$J_{w,f} = \frac{\Delta P - \eta_{rej,f}\pi_{fs}exp\left(\frac{J_{w,f}}{k_{ecp,f}}\right)}{\mu(R_m+R_f)} \tag{4}$$

268   where $J_{w,f}$ is the fouling water flux, $\eta_{rej,f}$ is the membrane rejection during the RO fouling

269   test, and $k_{ecp,f}$ is the overall mass transfer coefficient across the foulant layer and external

270   concentration polarization boundary layer. As shown by Eq. (5) $k_{ecp,f}$ is dependent on both

271   the external concentration polarization (ECP) and CECP at the feed side. Thus $k_{ecp,f}$ consists

272   of two terms, one is related to the mass transfer within the foulant layer on the membrane

273   ($k_{ecp,f*}$) and the other to the ECP boundary layer above the foulant layer ($k_{ecp,0}$).

274    $$\frac{1}{k_{ecp,f}} = \frac{1}{k_{ecp,0}} + \frac{1}{k_{ecp,f*}} = \frac{\delta}{D} + \frac{S_f}{D} = \frac{\overline{S_f}}{D} \tag{5}$$

275   where δ is the boundary layer thickness adjacent to the foulant layer and it can be estimated

276   from k_{ecp} for an empty channel [46]; S_f is the structural parameter of the foulant layer that has

277   an analogous definition to the membrane structural parameter [31]; $\overline{S_f}$ is the sum of δ and S_f

278   and is defined as the overall effective thickness of the CP boundary layer that incorporates both

279   CECP within the foulant cake layer and the external CP adjacent to the foulant layer. For the

280   calculation of R_f, a range of $\overline{S_f}$ from 125 μm to 719 μm (where 125 μm is the ECP boundary

281   layer thickness) was selected based on the nature of alginate fouling [47]. Clearly the CECP

282   effect is negligible when $\overline{S_f} = 125\ \mu m$. The selected range of $\overline{S_f}$ was rationalized via the

283   sensitivity analysis as detailed in Appendix B. The numerator of Eq. (4) represents the effective

284   driving force for RO during fouling and is used to calculate the RO effective driving force.

285

286 The R_f on the fouled FO membrane was calculated using π_{ds}, π_{fs}, and the experimentally

287 obtained parameters ($J_{w,f}$, $J_{s,f}/J_{w,f}$, R_m and S) based on the ORF model given below [37].

288 $$J_{w,f} = \frac{(\pi_{ds}-\pi_{fs})-F_{ecp,f}\left(\pi_{fs}+\frac{J_{s,f}}{J_{w,f}}\beta R_g T\right)-F_{dcp}\left(\pi_{ds}+\frac{J_{s,f}}{J_{w,f}}\beta R_g T\right)}{\mu(R_m+R_f)}$$ (6)

289 where the external concentration polarization (ECP) factor, $F_{ecp,f}$, at the feed side and dilutive

290 concentration polarization (DCP) factor, F_{dcp}, at the draw side are expressed by Eq. (7) and

291 Eq. (8), respectively.

292 $$F_{ecp,f} = exp\left(\frac{J_{w,f}}{k_{ecp,f}}\right) - 1$$ (7)

293 $$F_{dcp} = 1 - exp\left(-\frac{J_{w,f}}{k_{dcp}}\right) = 1 - exp\left(-\frac{J_{w,f}}{D/S}\right)$$ (8)

294 Eq. (6) incorporates the effect of reverse solute diffusion (i.e., J_s/J_w), internal concentration

295 polarization (included in F_{dcp}), and cake-enhanced concentration polarization (included in

296 $F_{ecp,f}$). The term $k_{ecp,f}$ in Eq. (7) was determined by Eq. (5) following similar approaches to

297 those for RO. Although a precise value of $\overline{S}_f$ was not determined in this study, the selected

298 range of $\overline{S}_f$ readily indicates the trend of the calculated R_f for FO and RO (also refer to

299 Appendix B). The numerator of Eq. (6) represents the effective driving force for FO during the

300 fouling test and is used to calculate the FO effective driving force. The effect of different

301 scenarios of $k_{ecp,f}$ on the calculated R_f and effective driving forces for FO and RO fouled

302 membranes will be evaluated and compared. ORF models show that the mass transfer

303 limitation for RO (Eq. (4)) only lies on the feed side but for FO (Eq. (6)) it lies on both the feed

304 and draw (permeate) sides which concurs with an earlier analysis [48]. As shown later ICP (or

305 k_{dcp}) at the draw side plays a significant role in determining the difference between FO and

306 RO fouling behaviours. It is important to note that the calculation of R_f for both FO and RO

307 fouled membranes (Eq. (4) and Eq. (6)) is based on the experimentally measured parameters,

13

308 which is essentially similar to the method for calculating clean membrane resistance R_m (or

309 clean membrane water permeability A) widely used in the research community [36, 41, 49, 50].

310

311 **3. Results and Discussion**

312 **3.1. Comparison of water flux performance between FO and RO**

313 For both FO and RO tests, the initial water flux was controlled at the same level of ~18 LMH

314 and the respective overall driving forces were maintained constant. Prior to fouling tests,

315 baseline tests without adding foulant in the FS were performed. The results show that baseline

316 fluxes for both FO and RO were almost constant during the entire test (Fig. S2 in Supporting

317 Information S3). Therefore, the flux decline during the fouling test is solely due to the addition

318 of foulant in the FS.

319

320 Fig. 1 shows the water flux behavior during FO and RO fouling tests and flux recovery after

321 membrane cleaning by water flushing. As shown in Fig. 1a, the water flux decline due to

322 membrane fouling in both FO and RO followed nearly the same trend. Similar observations

323 have been reported previously [19, 21, 24]. After the physical cleaning, water fluxes for both

324 FO and RO recovered significantly (Fig. 1b) with water flux recovery values of ~94% for FO

325 and ~96% for RO. Given the error bars the difference is not statistically significant. This

326 observation is different from that reported in previous studies in which flux recovery in FO

327 was generally much greater than that in RO [19-22, 24, 51]. Our results show that FO and RO

328 can have similar water flux decline trends during fouling and similar water flux recovery after

329 physical cleaning.

330

However, as introduced in Section 1, the water flux profiles alone do not reflect the extent of membrane fouling. The subsequent sections will provide an in-depth analysis of membrane fouling in both FO and RO via the comparison of R_f in both processes.
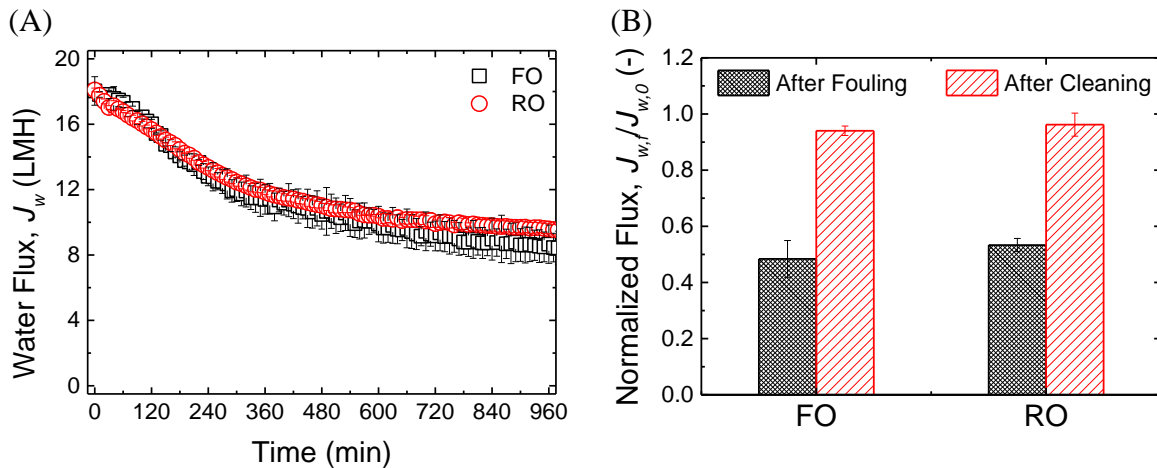
Fig.1. Comparison of FO and RO performance. (A) Water flux behavior during membrane fouling test, (B) water flux recovery after membrane cleaning. In the FO test DS was 1.5 M NaCl; in the RO test applied hydraulic pressure was 17.6 bar. Other fouling experimental conditions: FS contained 200 mg/L alginate, 45 mM NaCl and 5 mM $CaCl_2$; DS contained 1.5 M NaCl; no spacer was placed in FS flow channel, and a diamond net-type spacer was placed in DS flow channel; membrane active layer facing feed solution (AL-FS); cross-flow velocity in FS flow channel was 7.4 cm/s and that in DS flow channel was 11.1 cm/s. During membrane cleaning (surface flushing), the FS was replaced with DI water and cross-flow velocity increased to 29.6 cm/s for 30 minutes.

3.2. Comparison of fouling between FO and RO based on foulant resistance

Fig. 2 shows the foulant resistance R_f during FO and RO fouling calculated from the osmotic-resistance filtration models using the experimentally measured R_m of 3.26×10^{14} m^{-1}, S of 425 μm, $J_{w,f}$ from Fig. 1, specific reverse solute flux ($J_{s,f}/J_{w,f}$) for FO from Fig. S3 in Supporting Information S3, and rejection ($\eta_{rej,f}$) for RO from Fig. S4 in Supporting Information S3. The
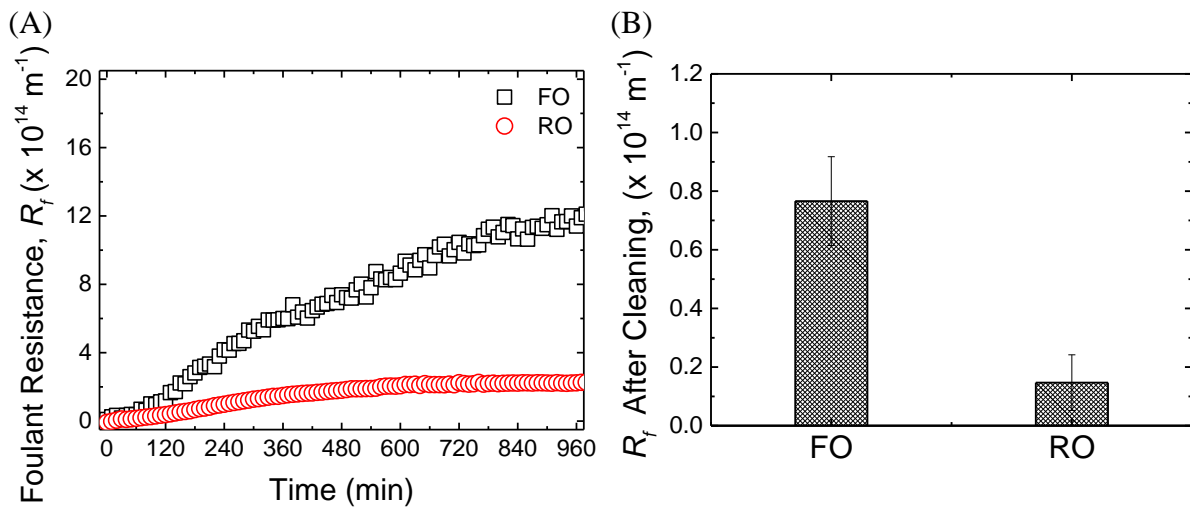
350   calculation of foulant resistance R_f incorporated the effect of cake-enhanced concentration

351   polarization as detailed in Appendix B. It was found that R_f for FO increased to a far greater

352   extent than that for RO with the progress of fouling (Fig. 2a). At the end of the 16-hour fouling

353   test, R_f for FO ($\sim 12.11 \times 10^{14}$ m^{-1}) was over 5 times that for RO ($\sim 2.27 \times 10^{14}$ m^{-1}). This

354   comparison of foulant resistances reveals that for our experimental conditions FO is more prone

355   to foulant accumulation than RO. More foulant accumulation in FO accords with the finding

356   of Tow et al. who reported that S_f for FO would be increasingly greater than RO [31]. A

357   sensitivity analysis of the effect of cake-enhanced concentration polarization on the calculated

358   R_f was performed for different scenarios with $\overline{S_f}$ varying from 125 to 719 μm. It was found

359   that the overall trend for all of the scenarios is similar to that in Fig. 2a (refer to Fig. B1 in

360   Appendix B).

361

362   Fig. 2B shows that after physical cleaning the residual foulant resistance R_f for FO ($\sim 0.77 \times 10^{14}$

363   m^{-1}) was also much greater than that for RO ($\sim 0.15 \times 10^{14}$ m^{-1}), although water flux recovery

364   for both processes was almost the same (Fig. 1B). This shows that basing conclusions solely

365   upon a comparison of water fluxes, as is common e.g. [19-22, 24, 51], can be misleading. The

366   trends of water flux (Fig. 1) and foulant resistance (Fig. 2) are reconciled in Section 3.4.

367

16

368

369

Fig. 2 – (A) Foulant resistance R_f during membrane fouling, and (B) Foulant resistance R_f after

membrane cleaning. R_f was calculated based on the osmotic-resistance filtration models (Eq.

(4) for RO and Eq. (6) for FO) using the experimentally measured water flux in Fig. 2, specific

reverse solute flux (J_s/J_w) from Fig. S3 in Supporting Information S3 for FO, rejection for RO

from Fig. S4 in Supporting Information S3, and basic membrane parameters (R_m and S), and

incorporating the cake-enhanced concentration polarization.

376

To further examine the extent of fouling, the fouled membranes were autopsied to ascertain the

foulant mass deposition density (m_f). As shown in Fig. 3a, at the end of the fouling test the

amount of alginate depositing on the unit area of membrane surface for FO (~2.25 mg/cm^2)

was nearly 2 times of that for RO (~1.24 mg/cm^2). Interestingly, the specific foulant resistance

(R_f/m_f) as shown in Fig 3b indicates that the unit amount of alginate depositing on the

membrane for FO caused greater hydraulic resistance than that for RO; R_f/m_f for FO

(~5.40×10^{10} m/mg) is approximately 3 times of that for RO (~1.85×10^{10} m/mg).

384

(A)   (B)

17
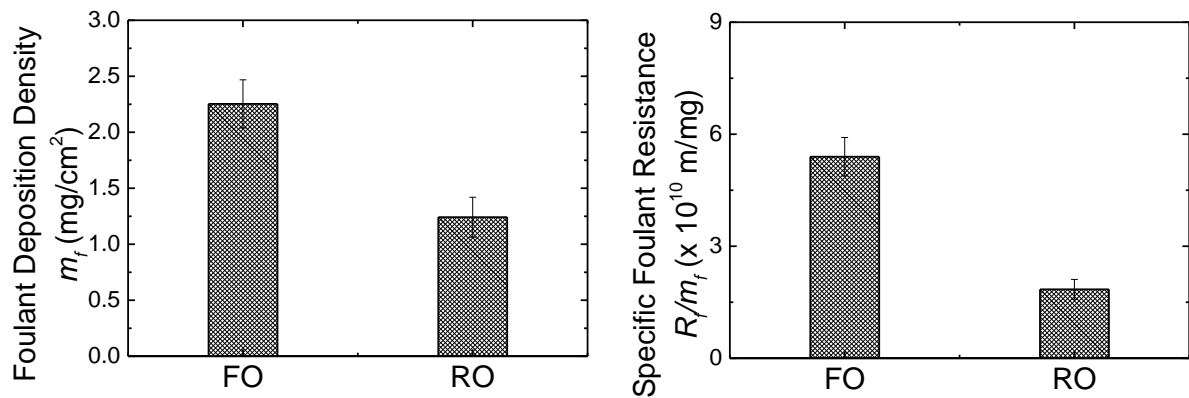
Fig. 3 – (A) Foulant deposition density, m_f; (B) Specific foulant resistance R_f/m_f. To calculate the R_f/m_f, R_f was the value at the end of fouling test collected from Fig. 2.

That greater values of both m_f and R_f/m_f were observed for FO is contradictory to some previous studies in which it is generally claimed that the foulant layer is less compacted in FO than RO owing to the lack of hydraulic pressure in FO [19, 21-24]. Thus experiments specifically designed to investigate the effect of hydraulic pressure on the compaction of the foulant layer were undertaken, which is discussed later in Section 3.3.

With regard to the finding of greater values of both m_f and R_f/m_f for FO (in comparison to RO) it is noted that this does accord with the findings of Song and Elimelech [52] who modelled particle transport rates toward a nonporous membrane. They found a significant increase in particle deposition upon an increase in salt concentration. Now in FO there is a significantly higher salt concentration adjacent to the membrane due to reverse salt diffusion and so greater particle deposition can be anticipated. Using experimental evidence provided by the work of Sim et al. [53] it was shown that an increase in ionic strength of the feed solution leads to increases in cake thickness and decreases in cake porosity which accords exactly with the experimental findings reported above for FO. The mechanisms for fouling differences in FO and RO are discussed in more detail in section 3.4.
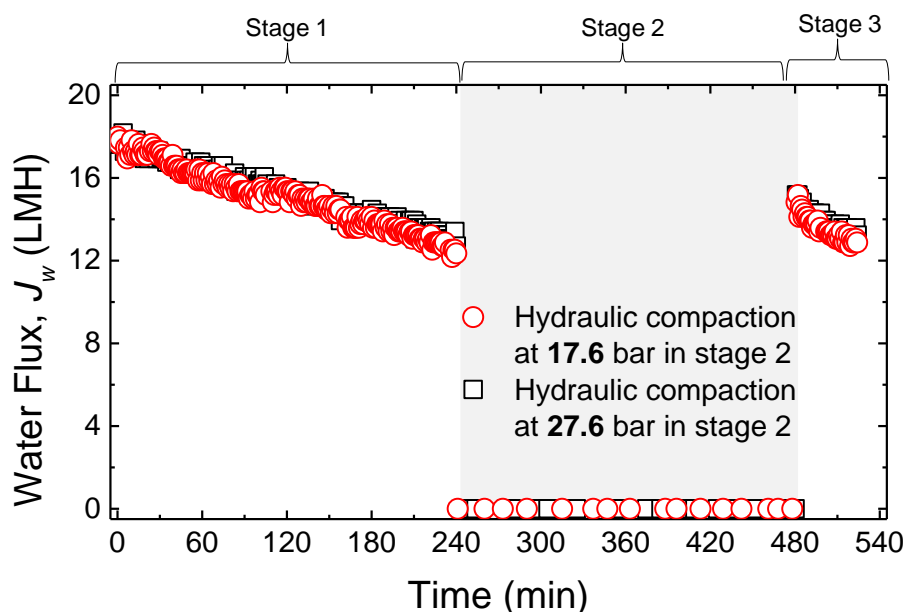
3.3. Effect of hydraulic pressure on the compaction of foulant layer

405

406   As shown in Fig. S5 in Supporting Information S4, the experiment was divided into three stages:

407   (1) foulant layer development stage, (2) solely hydraulic pressure compaction stage, and (3)

408   performance re-evaluation stage. The test results are shown in Fig. 4. The first stage is the

409   initial 4-hour constant-pressure (~17.6 bar) RO fouling test, at the end of which a foulant layer

410   had formed on the membrane; the water flux had declined over 30%. In the second stage, the

411   permeate valve was closed to ensure the permeate water flux was zero, thus eliminating the

412   flux-induced hydrodynamic drag compaction and only leaving the hydraulic pressure

413   (maintained at ~17.6 bar or elevated to ~27.6 bar) to "compact" the foulant layer for another 4

414   hours. In the third stage, the permeate valve was opened again and the permeate water flux was

415   re-measured under the same pressure used in the first stage (~17.6 bar).

416

417   If the hydraulic pressure plays a more critical role in the "compaction" of the foulant layer than

418   the water permeation drag force as previously claimed [24], then one would have expected to

419   find upon reopening of the permeate valve that the hydraulic resistance of the foulant layer (R_f)

420   had increased and the water flux had decreased. However, the opposite was found. As shown

421   in Fig. 4 the water flux was elevated significantly after the fouled membranes had been solely

422   "compacted" by the hydraulic pressure in the second stage. Importantly it was found that the

423   level of the water flux elevation was independent of the pressure used to solely "compact" the

424   foulant layer. The elevated water flux is likely to be due to the removal of some of the foulant

425   layer by the cross-flow shear force in the absence of flux-induced drag. Our results suggest

426   that it is the hydrodynamic drag force due to flux rather than the hydraulic pressure *per se* that

427   plays a critical role in the compaction of the alginate fouling layer.

19

429

Fig. 4 – Effect of hydraulic pressure on the compaction of foulant layer. Water flux at different

stages is shown. Stage 1 is normal RO operation at 17.6 bar; in stage 2 foulant layer is

compacted only by hydraulic pressure at either 17.6 bar or 27.6 bar in which the permeate valve

is closed and permeate water flux is zero; in stage 3 the permeate valve is reopened and the

water flux is re-evaluated at 17.6 bar after the sole hydraulic compaction in stage 2. Other

experimental conditions: FS contained 200 mg/L alginate, 45 mM NaCl and 5 mM $CaCl_2$; no

spacer is placed in FS flow channel; cross-flow velocity in FS flow channel is 7.4 cm/s.

The above findings are in agreement with other previous studies [32, 54, 55]. When studying

RO and NF membrane fouling by humic acid [54], Tang and Leckie observed a limiting flux

that is independent of applied pressures (initial water fluxes) and membrane properties,

suggesting that the foulant layer compaction might not be dominated by pressure but by flux;

otherwise a limiting flux would not be observed. During the investigation of RO membrane

fouling under constant-flux operation (see Fig. S6 in Supporting Information S4) and [32],

Fane et al. found no clear difference in TMP profiles with varying feed pressure for either silica

or alginate fouling as long as the water flux was maintained constant. They concluded that cake

20

446 filtration is related to the differential pressure across the fouling layer that is physically related

447 to flux (Eq. (4)) rather than to the absolute pressure itself [56]. In a recent study Tow and

448 Lienhard found that alginate gel compaction by high feed hydraulic pressure does not occur

449 and suggested that other explanations should be sought for FO's fouling resistance relative to

450 RO [55]. In the following sections we will explore further the mechanisms governing the

451 different fouling behaviours between FO and RO observed in this study.

452

453 **3.4. Mechanisms for the different fouling behaviours between FO and RO**

454 **3.4.1. ICP self-compensation effect**

455 The difference in foulant accumulation between FO and RO can be attributed primarily to the

456 different responses of their driving forces to the water flux. For FO the effective osmotic

457 driving force is significantly influenced by the ICP that is exponentially proportional to the

458 water flux [35, 36]. A small variation of water flux can result in a significant variation of ICP

459 and thus effective driving force [36]. Fig. 5 shows the effective driving forces for FO and RO

460 during the fouling tests. Despite the same effective driving force at the beginning of fouling

461 tests, the effective driving force for FO increased significantly with the progress of fouling test,

462 while that for RO slightly decreased. At the end of fouling test the effective driving force for

463 FO became nearly three times of that for RO. In an earlier study of modelling the effective

464 driving force for FO and RO under the same extent of fouling, Lay et al. also found that the

465 effective driving force for FO was greater than that for RO [29].

466
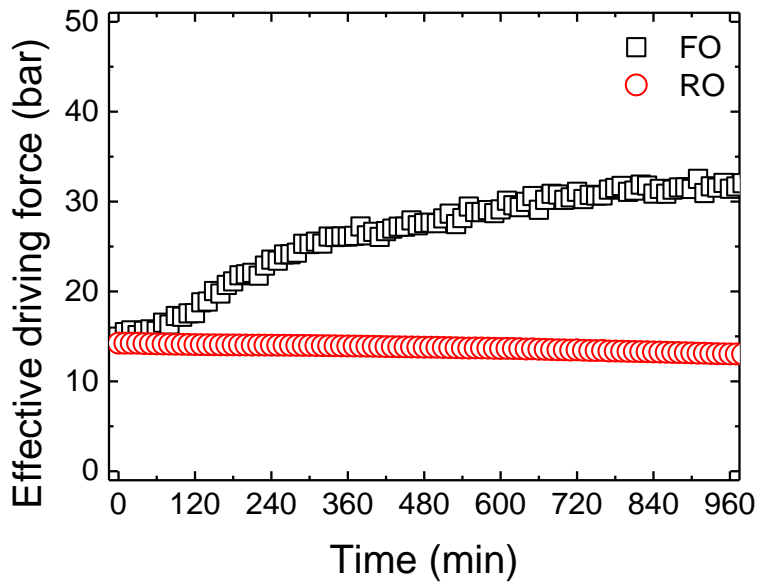
467

468 Fig. 5 – Comparison of effective driving force in FO and RO during the fouling test. Effective

469 driving force is the numerator of osmotic-resistance filtration models (Eq. (4) for RO and Eq.

470 (6) for FO) and is calculated using the experimentally obtained water flux in Fig. 2, specific

471 reverse solute flux (J_s/J_w) from Fig. S3 in Supporting Information S3 for FO, rejection for RO

472 from Fig. S4 in Supporting Information S3, and basic membrane parameters (R_m and S), and

473 incorporating the cake-enhanced concentration polarization.

474

475 The progressively increased effective driving force in FO is due to the ICP self-compensation

476 effect [36, 37]. That is, the decreased water flux due to membrane fouling results in a decrease

477 in ICP, which in turn leads to an increase in the effective osmotic driving force. The different

478 evolution of fouling in FO and RO is elaborated through simulation as discussed in detail in

479 Section 3.5 and as shown in Fig. 8 later. Here a pictorial explanation is given. Although there

480 are not discreet steps, one can view the evolution of the flux decline as consisting of a number

481 of components as depicted in Fig. 6A. The increase in the effective driving force in FO leads

482 to partial flux compensation which in turn leads to greater foulant accumulation. More

483 accumulation leads to a further decrease in water flux and with the decreased water flux (and

484   the consequent ICP self-compensation) the process continues until there is a balance between

485   foulant being convected to the surface and foulant being removed by crossflow.

486

487   In contrast, the effective driving force for RO (i.e., the difference between the hydraulic

488   pressure and the osmotic pressure) responds much less significantly to the change of water flux,

489   noting that in RO only external CP changes with flux but hydraulic pressure is maintained

490   constant. It could even decrease with the progression of fouling due to increased cake-enhanced

491   concentration polarization (Fig. 6B). Thus, the compensation for partial flux decline is much

492   weaker or does not exist for RO. Consequently, the increase of foulant resistance for RO is

493   much smaller than that for FO (Fig. 2A) and the foulant deposit in RO is smaller than FO (Fig.

494   3A).

495

496   The evolution of foulant accumulation (R_f) can also be explained mathematically by

497   differentiating the water flux equation $J = F/\mu R$ with respect to time (t), which is easy to show

498   that

499    $$\frac{dR/dt}{R} = \frac{(-dJ/dt)}{J} + \frac{dF/dt}{F}$$ (9)

500   where J is water flux, F is driving force, and R is resistance. Thus the relative increase in

501   resistance at any point during the evolution of the resistance is the sum of the relative flux

502   decline and the relative increase in driving force. In the case of RO the third term is negligible

503   or very small but in the case of FO it is not. Therefore for the similar water flux decline profile,

504   the increase in resistance for FO is increasingly greater than RO.

505

506   It is well known that for a compressible filter cake that the porosity at the bottom, i.e., nearest

507   the support (it is membrane in our case), is lowest. This is because the bottom layers of the

508   cake have to support the drag forces imparted on the top layer of the cake. If there is more drag

23

509 (due to larger deposit and R_f as in FO at compensated partial flux), the bottom of the cake is

510 more compressed. Our measured specific cake resistance is the cake average value, but this

511 may be dominated by the effect of the bottom layer. This offers a partial explanation for the

512 greater specific cake resistance for FO than RO (Fig. 3B) or more exactly an explanation for

513 augmentation of the higher specific cake resistance. This might also explain that, under the

514 same surface flushing conditions, the residual foulant resistance for FO fouled membrane was

515 greater than RO fouled membrane (Fig. 2B), since the bottom cake layer might dominate the

516 overall specific cake resistance. A second reason for higher specific resistance in FO is that

517 the diffusiophoretic gradient is higher within the cake layer [57] due to reverse solute diffusion

518 and as noted in this previous study this could lead to cake compaction by diffusiophoresis (DP);

519 this will be discussed further in Section 3.4.3.
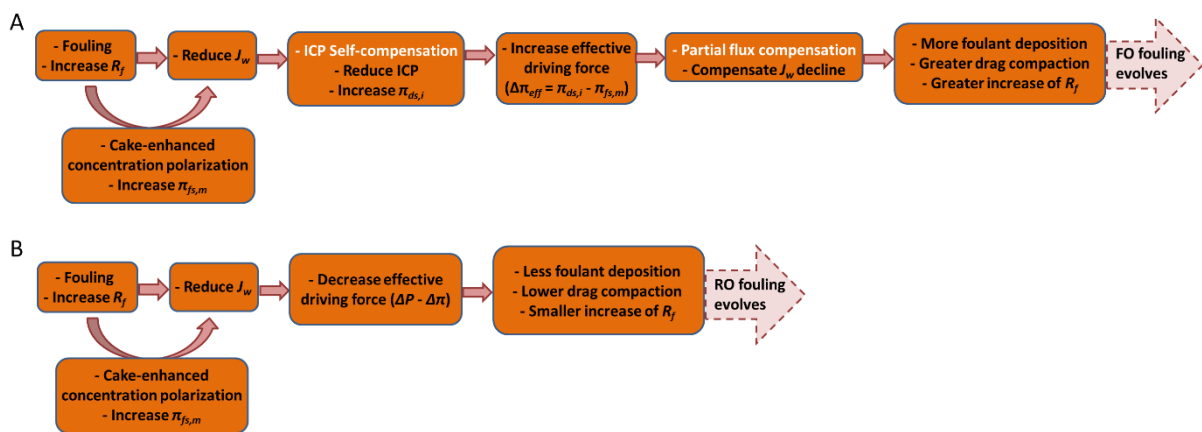
520

521 Fig. 6 – Evolution of membrane fouling in (A) FO and (B) RO. The relationship linking fouling,

522 water flux, ICP self-compensation, cake-enhanced concentration polarization (CECP), and

523 effective driving forces in FO and RO is schematically illustrated.

524

525 **3.4.2. Cake-enhanced concentration polarization (CECP)**

526 The results in Fig. 5 on the analysis of effective driving force also suggest that cake-enhanced

527 concentration polarization (CECP) might play a less important role in FO in the AL-FS

528 orientation compared to that in RO for the alginate fouling in this study. For RO, CECP could

529   result in the decrease of effective driving force that further aggravates the decrease of water

530   flux. However, for FO, CECP would not change the trend where the effective driving force

531   tends to increase with the progress of fouling. The reasoning again relates to the ICP self-

532   compensation effect – the decreased ICP at the draw side due to the decrease of water flux by

533   fouling was much more significant than the cake-enhanced CP at the feed side in this study.

534   This was further demonstrated through sensitivity analysis for a wide range of scenarios - see

535   Fig. B1b in Appendix B. This shows that the increase of effective driving force for FO could

536   be moderately slowed down at an increased CECP, but the overall trend (effective driving force

537   for FO significantly > RO) remains unchanged as long as the fouling continues to lead to an

538   increase of foulant resistance (R_f). This finding supports an earlier study on the modelling of

539   the effect of feed concentration on FO water flux, where She et al. suggested that CECP might

540   not be important for FO in the AL-FS membrane orientation due to the strong ICP self-

541   compensation effect [37].

542

543   **3.4.3. Reverse solute diffusion (RSD)**

544   The reverse diffusion of draw solute into the FS can influence the fouling behaviour (either

545   increasing or decreasing fouling) due to the change of local feed solution chemistry near the

546   FO membrane surface, which has been identified to be a unique fouling mechanism for

547   osmotically driven membrane processes [37, 43, 44]. In the current study the reverse diffusion

548   of NaCl from DS into FS would elevate the ionic strength of FS. As shown in Fig. 7, it was

549   estimated, based on the approach reported previously [58, 59], that the local ionic strength near

550   the active layer surface was elevated from ~98 mM at the beginning to ~167 mM at the end of

551   the fouling test due to both CECP and reverse solute diffusion (RSD). In comparison, during

552   the RO fouling test the bulk FS ionic strength is constant (~60 mM) and the local ionic strength

553   near the active layer surface was elevated from ~86 mM to ~117 mM due to CECP. It has been

554   reported that with an increased ionic strength, the alginate fouling rate reduces when the feed

555   solution has a high Ca^{2+} concentration ($>$ 1 mM) [60, 61] due to the reduced binding affinity

556   between Ca^{2+} and carboxyl units of the organic compounds [60-63]. Owing to the relatively

557   high Ca^{2+} concentration (5 mM) in the feed solution in the present study, it was expected that

558   the increased ionic strength at the feed side in FO due to reverse diffusion of NaCl could lead

559   to a decreased specific cake resistance. However experimental results in Fig. 2 show that the

560   specific cake resistance as well as the overall foulant resistance was greater for FO compared

561   with RO. This suggests there would be other reasons. In addition to the ICP self-compensation

562   as discussed in Section 3.4.1, another potential contributing effect is diffusiophoresis (DP) [57].

563

564   In FO, due to RSD, there would be a steeper concentration gradient of salinity across the foulant

565   layer, which aligns with estimates in Fig 7. This would invoke a stronger diffusiophoresis (DP)

566   effect in FO than RO, particularly if the feed solution is of low salinity. This stronger effect in

567   FO may not only lead to a great specific resistance but could also augment the degree of

568   deposition. Whilst the greater foulant load in FO compared to RO is definitely due in part to

569   the decrease in the intensity of ICP with time, and hence the increase in effective driving force,

570   it may be augmented by DP. Previous work has shown that the critical flux for a feed consisting

571   principally of humic acid had a lower value with an RO membrane compared to the value for

572   a UF membrane. (Taheri paper JMS 2015). Now this was partially attributed to DP because

573   for the RO membrane (unlike the UF one) salt gradients would be established. The plateau

574   fluxes in Fig. 1 (which can be taken as a measure of the critical fluxes) are lower for FO than

575   RO by around 10-15% and this accords with DP having a potential role in determining the net

576   flux of foulants towards the membrane surface.

577

578
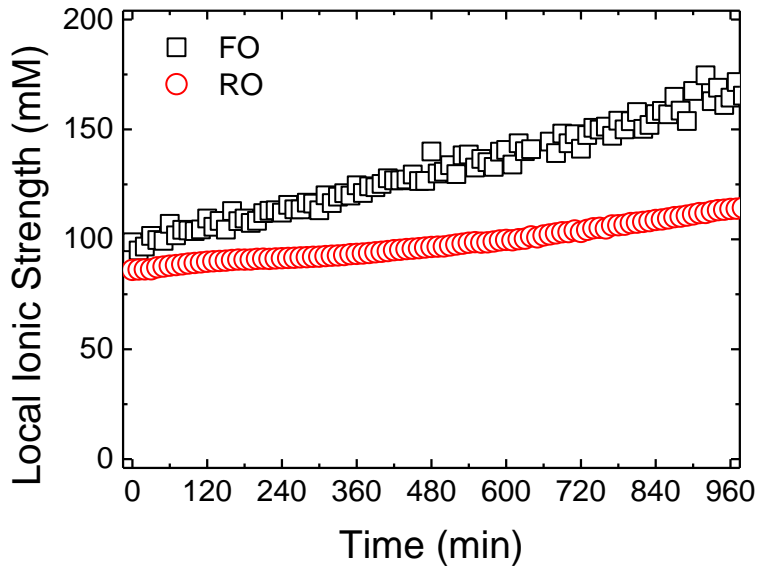
Fig. 7 – Estimated local ionic strength near the membrane active layer surface for FO and RO

during the fouling test. The calculation of local ionic strength followed the method reported

previously [58, 59] incorporating cake-enhanced concentration polarization.

3.5. Implications

The above experimental results show that although FO is more prone to fouling in terms of

more foulant accumulation and greater foulant hydraulic resistance than RO, the water flux in

FO might be more stable against fouling, which could enable FO to be a more resilient process

in some applications. This is further elaborated in this section by the simulation of FO and RO

water fluxes as a function of the extent of fouling (i.e., foulant resistance) in Fig. 8. The slope

of Fig. 8 was mathematically derived in Appendix C to further help the analysis of the fouling

behaviour. For the same extent of fouling (i.e., at the same R_f when $R_f > 0$) it is apparent that

the water flux for FO is intrinsically higher than that for RO, demonstrating the superiority of

FO to RO in terms of water flux performance. However, the same extent of fouling will not be

a stable condition in a practical operation. This is because a higher flux in FO under such

conditions would bring more foulants towards the membrane and lead to a greater

hydrodynamic drag force, which would result in more foulant accumulation in FO and in turn

27

596 more flux decline, as exhibited in our experimental observations (see Sections 3.1 and 3.2). Fig.

597 8 also shows that at the same level of water flux during fouling tests the foulant resistance for

598 FO has to be greater than that for RO. This concurs with our experimental observations in

599 Section 3.2. As illustrated in Fig. 8, in some cases FO can exhibit higher flux even at more

600 severe fouling (e.g., water flux of FO at foulant resistance of $R_{f,2}$ is greater than that of RO at

601 $R_{f,1}$).
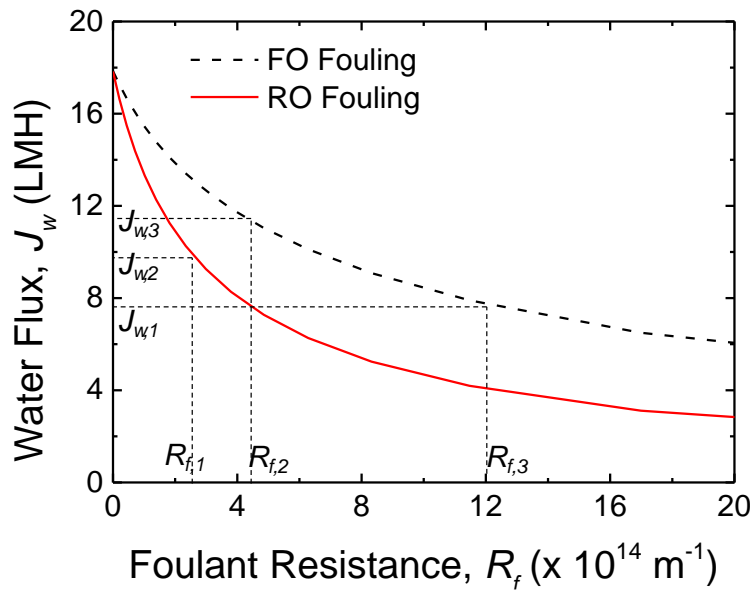
602

603 Fig. 8.   Simulation of water flux of FO and RO as a function of foulant resistance. The

604 simulation is based on the osmotic-resistance filtration models (Eq. (4) and Eq. (6)) assuming

605 that membrane fouling only leads to the increase of R_f while other membrane parameters (solute

606 permeability coefficient B value and structural parameter S value) are unchanged. Cake-

607 enhanced concentration polarization (CECP) is considered in the simulation by assuming $\bar{S}_f$

608 increases from 125 μm to 500 μm. For the clean membrane the R_m is 3.26×10^{14} m^{-1}, the B

609 value is 4.47×10^{-7} m/s, and the S value is 425 μm.

610

611 During membrane cleaning, the water flux for FO can be recovered to a higher level than RO

612 even though the fouled FO membrane is not cleaned to the same extent as the fouled RO

613 membrane. This point is illustrated in Fig. 8. Considering that the foulant resistance for FO is

28

614 reduced from $R_{f,3}$ to $R_{f,2}$ after membrane cleaning (Fig. 8), the water flux for FO will still be

615 greater than that for RO when the foulant resistance is reduced from $R_{f,2}$ to $R_{f,1}$ in Fig. 8. Again

616 this indicates that the change of water flux in FO in response to a given change of foulant

617 resistance (i.e. fouling) is much less than that in RO. This also explains why fouling

618 reversibility, based on measured water fluxes, appears to be more effective for FO than RO

619 [19-25, 27]. This is not due to the foulant layer in FO being less compacted (indeed on the

620 contrary we found the specific resistance to be higher for FO) but because the change in ICP

621 (and thus the change in effective driving force) in FO leads to a higher flux in the presence of

622 residual fouling.

623

624 The above modelling does not incorporate the influence of diffusiophoretic deposition (DP).

625 As elegantly illustrated in Fig.9 of their paper, Guha et al [57] showed that for filtration-based

626 particle deposition leading to convective cake formation one can often expect filtration-based

627 ion concentration polarization which leads to diffusiophoretic movement augmenting particle

628 deposition and this in turn creates both a greater level of cake formation and compaction, and

629 further enhanced ion concentration polarization. Thus there is a positive feed-back loop further

630 enhancing fouling.

631

632 In summary, the advantage of greater water flux stability of FO over RO is due to the ICP self-

633 compensation effect for FO that can result in a partial water flux compensation and leverage

634 the water flux decline by increasing the effective driving force. Our results suggest that,

635 contrary to earlier reports, FO does not benefit from less foulant compression due to its low

636 hydraulic pressure operation. While ICP is generally regarded as a detrimental effect for FO,

637 the current study reveals that ICP can also have an upside in that it helps to maintain water flux

638 stability. An interesting corollary to this is that the quest for FO membranes with smaller and

639　　smaller S values to reduce ICP needs to consider whether there is an optimal S value that

640　　balances the magnitude of flux decline and the resilience that the ICP compensation imparts

641　　upon the system.

642

643　　**4. Conclusions**

644　　In this study the differences in membrane fouling between FO and RO were explored under

645　　comparably controlled experimental conditions in which the apparent driving forces for FO

646　　and RO were maintained constant. Sodium alginate was the foulant. It was found that:

647　　1. Water flux decline during both FO and RO fouling tests followed broadly the same trend

648　　　　and water flux recovery after membrane cleaning for both FO and RO reached a similar

649　　　　level. However, the driving forces of FO and RO respond differently to the progression of

650　　　　fouling and as a result the foulant resistance for FO was increasingly greater than that for

651　　　　RO.

652　　2. Membrane autopsy after the fouling tests showed that more foulant had been deposited on

653　　　　the FO fouled membrane than the RO fouled membrane. Also, the specific foulant

654　　　　resistance was greater with FO than RO.

655　　3. The dominant reason for the higher fouling propensity in FO is due to the change of ICP

656　　　　and effective driving force in response to the evolution of fouling; it is true for all systems

657　　　　with manifest ICP.

658　　4. Calculations suggest that CECP does not play an important role in flux decline in FO due

659　　　　to the dominance of the ICP self-compensation effect.

660　　5. The reverse diffusion of draw solute into feed solution could also influence fouling in FO

661　　　　in two ways. Firstly directly as a result in the change of feed solution chemistry, an effect

662　　　　that is strongly dependent on the draw solution properties. Secondly RSD will also

663　　　　influence the salinity gradient across the FO foulant layer. This gradient will be greater in

30

664   FO than the corresponding one for RO and probably led to diffusiophoresis (DP). The role

665   of DP in FO is worthy of further investigation.

666   6. No evidence was found that hydraulic pressure in RO plays a critical role in the compaction

667   of alginate fouling layers. Furthermore the generally observed high flux reversibility of

668   FO after membrane cleaning is probably due to the change of ICP (and thus effective

669   driving force) in response to fouling rather than the lack of compaction due to hydraulic

670   pressure.

671   7. Overall and not withstanding its higher fouling propensity, FO was found to exhibit higher

672   flux stability against membrane fouling. Excluding those applications where the reverse

673   salt flux generates additional fouling FO is potentially a more resilient process than RO.

674

683

684   **Appendix A. Derivation of osmotic-resistance filtration model for RO**

685   The osmotic-resistance filtration model of Eq. (A1) is originally derived for osmotically driven

686   membrane processes and differentiates all the driving forces incorporating concentration

687   polarization and reverse solute diffusion [37].

688    $$J_w = \frac{(\pi_{ds}-\pi_{fs})-F_{ecp}\left(\pi_{fs}+\frac{J_s}{J_w}\beta R_g T\right)-F_{dcp}\left(\pi_{ds}+\frac{J_s}{J_w}\beta R_g T\right)}{\mu R_m}$$ (A1)

689 where F_{ecp} and F_{dcp} are the concentrative external concentration polarization (ECP) factor at

690 the feed side and dilutive concentration polarization (DCP) factor at the draw side respectively.

691 They are expressed by Eq. (A2) and Eq. (A3).

692 $$F_{ecp} = exp\left(\frac{J_w}{k_{ecp}}\right) - 1 \tag{A2}$$

693 $$F_{dcp} = 1 - exp\left(-\frac{J_w}{k_{dcp}}\right) = 1 - exp\left(-\frac{J_w}{D/S}\right) \tag{A3}$$

694 Eq. (A1) is also applicable for RO and can be expressed as Eq. (A4) considering the direction

695 of water flux and solute flux as well as the redefinition of signs to represent the parameters for

696 RO.

697 $$J_w = \frac{\Delta P - (\pi_{fs} - \pi_p) - F_{ecp}\left(\pi_{fs} - \frac{J_s}{J_w}\beta R_g T\right)}{\mu R_m} \tag{A4}$$

698 At equilibrium DCP does not exist in RO and the specific solute flux ($\frac{J_s}{J_w}$) can be correlated to

699 the permeate concentration (c_p) by Eq. (A5).

700 $$c_p = \frac{J_s}{J_w} \tag{A5}$$

701 Inserting Eq. (A2) and Eq. (A5) into Eq. (A4) yields the expected equation:

702 $$J_w = \frac{\Delta P - (\pi_{fs} - \pi_p)exp\left(\frac{J_w}{k_{ecp}}\right)}{\mu R_m} \tag{A6}$$

703 By assuming that the concentration and osmotic pressure follow the van't Hoff equation, the

704 solute rejection in RO can be expressed below.

705 $$\eta_{rej,f} = 1 - \frac{c_p}{c_f} = 1 - \frac{\pi_p}{\pi_f} \tag{A7}$$

706 Inserting Eq. (A7) into Eq. (A6) yields

707 $$J_w = \frac{\Delta P - \eta_{rej}\pi_{fs}exp\left(\frac{J_w}{k_{ecp}}\right)}{\mu R_m} \tag{A8}$$

708

Appendix B. Sensitivity analysis of the effect of cake-enhanced concentration polarization

(CECP) on the calculated values of foulant resistance R_f

This section shows the results of a sensitive analysis in which the influence of assumed levels of cake-enhanced concentration polarization (CECP) on the calculated R_f for FO and RO were explored. R_f was calculated for the following four scenarios using the experimentally measured data (i.e., J_w, J_s/J_w, R_f, S, π_{ds} and π_{fs}).

- Case (1): ECP at the feed side is neglected (i.e., assuming $\overline{S_f} = 0$ in Eq. (5)).

- Case (2): ECP at the feed side is considered but CECP is neglected (i.e., assuming $S_f = 0$ and $\overline{S_f} = \delta$ in Eq. (5); using $\overline{S_f}$ of 125 μm that is estimated for empty flow channel following the method reported elsewhere [46]).

- Case (3): CECP is considered and S_f is the same for both FO and RO (i.e., assuming that $\overline{S_f}$ for both FO and RO increases at the same rate with the progress of fouling test from 125 μm at the beginning of fouling test to 422 μm at the end of fouling test).

- Case (4): CECP is considered and S_f for FO becomes increasingly greater than that for RO based on the analysis of Tow et al. [31] (i.e., $\overline{S_f}$ for FO increases faster with the progress of fouling than that for RO; specifically it was assumed that $\overline{S_f}$ for FO increases from 125 μm to 719 μm whilst that for RO increases from 125 μm to 422 μm during the fouling tests).

As shown in Fig. B1a, for all the scenarios R_f for both FO and RO increased with the progress of fouling test. Moreover, although the increase of concentration polarization from Case (1) to (4) at a fixed time could decrease the calculated R_f for both FO and RO, for all scenarios R_f for FObecomes increasingly greater than that for RO. Note that for Case (4) the selected range of $\overline{S_f}$ for FO from 125 μm to 719 μm over the testing period approaches an extreme condition in which a further faster increase in $\overline{S_f}$ (i.e. a more severe rate of foulant accumulation) would

33

733   result in a decrease in the calculated R_f (see Fig. B1c for Case (5)) which is unrealistic. In

734   addition, the assumption of a faster increase of $\bar{S}_f$ for FO in Case (4) has already suggested that

735   foulant accumulation for FO is more severe than that for RO [31]. As there is much greater R_f

736   for FO with the progress of fouling, these results further corroborate our observation that FO

737   has a greater fouling propensity than RO even under the extreme conditions considered here.

738   Although a more valid method needs to be developed to determine the accurate $\bar{S}_f$ value, the

739   sensitive analysis with $\bar{S}_f$ varying within the boundary conditions can clearly demonstrate that

740   R_f for FO is always greater than RO under the experimental conditions in the current study.
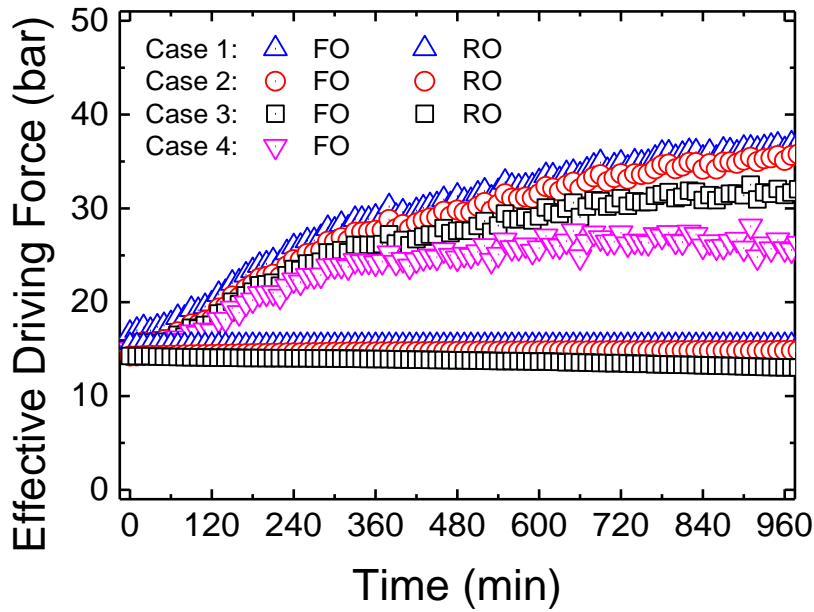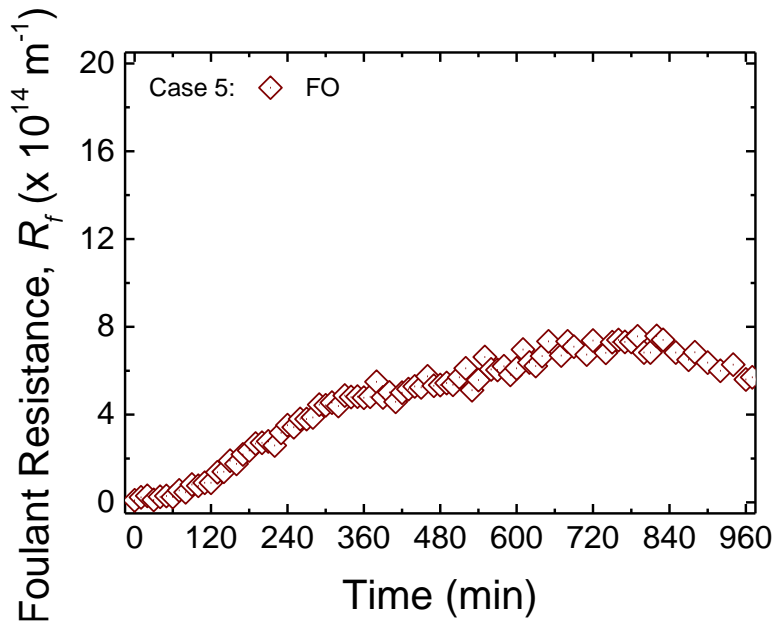
741

742   (a)

743
744
745
746   (b)

(c)
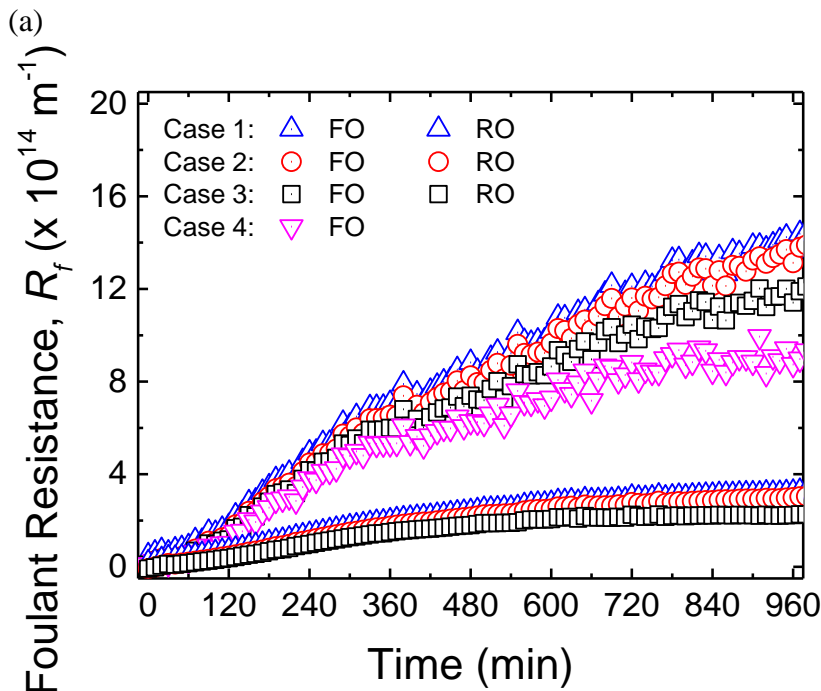
752 Fig. B1 – Calculated foulant resistance (R_f) (a) and effective driving force (b) for FO and RO
753 based on the osmotic-resistance filtration model in different scenarios: (1) cake-enhanced
754 concentration polarization (CECP) is neglected (i.e., assuming that the ECP boundary layer
755 thickness (δ) is zero), (2) CECP is considered but cake-enhanced concentration polarization is
756 neglected (i.e., using δ of 125 μm that is estimated for empty flow channel following the
757 method reported elsewhere [46]), (3) CECP is considered and the foulant layer structural
758 parameter (S_f) is the same for both FO and RO (i.e., $(\delta + S_f)$ for both FO and RO increases at
759 the same rate with the progress of fouling test from 125 μm at the beginning to 422 μm at the
760 end of fouling test), and (4) CECP is considered and the foulant layer structural parameter (S_f)
761 for FO becomes increasingly more greater than that for RO (i.e., $(\delta + S_f)$ for FO increases
762 faster with the progress of fouling than that for RO; $(\delta + S_f)$ for FO increases from 125 μm to
763 719 μm, while that for RO increases from 125 μm to 422 μm). For the calculation, the

764 experimentally obtained clean membrane resistance R_m is 3.26×10^{14} m^{-1} and structural

765 parameter S is 425 μm. (c) foulant resistance (R_f) for case (5) when the $\overline{S_f}$ has a faster increase

766 than that in case (4).

767

768 Fig. B1b shows the effective driving force for FO and RO. For all the Cases the effective

769 driving force for FO increased with the progress of fouling test and became increasingly greater

770 than that for RO. In contrast to FO, the effective driving force for RO behaved differently for

771 different scenarios: it maintained constant for Case (1), increased gradually with fouling test

772 for Case (2), and decreased gradually with fouling test for Case (3). Although the increase of

773 concentration polarization from Case (1) to Case (4) led to the decrease of effective driving

774 force for both FO and RO at a fixed time of fouling test, the effective driving force for FO was

775 always increasing with the fouling test and becoming increasingly greater than that for RO.

776 This suggests that (1) the different response of the effective driving force to fouling test

777 between FO and RO is the major reason for their different fouling behaviours, and (2) CECP

778 for FO plays a much less important role in flux decline than it does for RO.

779

780 Fig. B2 shows the calculated specific foulant resistance (R_f/m_f) using the experimentally

781 measured foulant deposition density (m_f) and calculated R_f in Case (4) that is under the

782 extreme conditions. Interestingly, the specific foulant resistance (R_f/m_f) for FO is still

783 consistently greater than RO even under the case of extreme conditions.

784
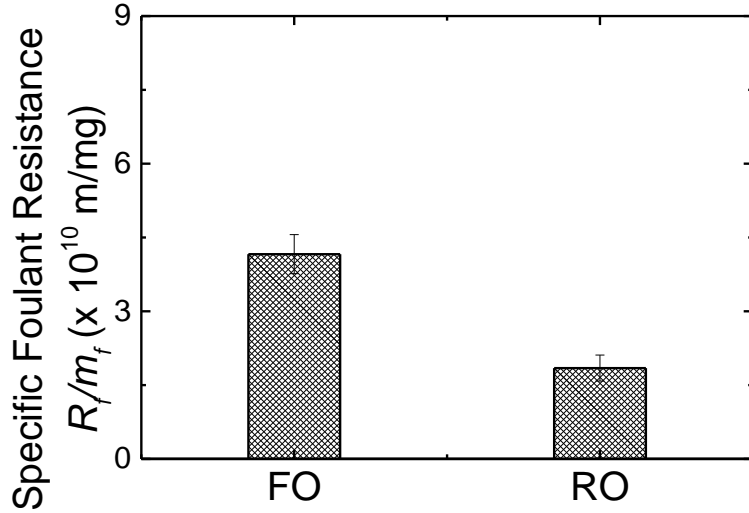
785

786 Fig. B2 – Specific foulant resistant (R_f/m_f) for FO and RO. R_f/m_f was calculated using the R_f
787 from Fig. B1a in Scenario (4) and the experimentally measured m_f in Fig. 3A.
788

Appendix C. Mathematic derivation of flux decline with respect to foulant accumulation

790 For simplicity we write $R = R_m + R_f$ in the development of (C2) and (C3). We ignore feed

791 side and draw side external concentration polarization for FO (i.e., equation (C2)) and feed side

792 external concentration polarization for RO (i.e., equation (C3)).

793 For FO:
$$J = \frac{\pi_{ds}.\exp\left(-\frac{J}{k_{dcp}}\right)-\pi_{fs}}{\mu R} \tag{C1}$$

794 Hence for FO the rate of flux decline with respect to fouling is:

795
$$\frac{dJ}{dR_f} = \frac{-\left(\pi_{ds}.\exp\left(-\frac{J}{k_{dcp}}\right)-\pi_{fs}\right)}{\mu R^2} \Bigg/ \left[1 + \pi_{ds}.\exp\left(-\frac{J}{k_{dcp}}\right)\Big/k_{dcp}R\right] \tag{C2}$$

796 However for RO the corresponding equation to (C2) is:

797
$$\frac{dJ}{dR_f} = \frac{-\Delta P}{\mu R^2} \tag{C3}$$

798 At the beginning of both experiments $R \approx R_m$ and the only difference between (C2) and (C3),

799 is the denominator in square brackets in (C2). These expressions are related to the gradient of

800 the curves in Fig. 8. The clear implication is that for a given deposition of foulant (equating to

801 a given ΔR) the change in flux will be smaller in FO than in RO. Now foulant accumulation

37

802   can be expected to continue at a decreasing rate until there is a balance between deposition, by

803   convective flow to and through the membrane, and removal by shear [64]. Now given that flux

804   is declining more slowly with respect to a given amount of foulant accumulation in FO than

805   RO there will naturally be a greater amount of foulant deposition in FO before the limiting flux

806   is reached.

807

808   **Appendix D. Supplementary material**

809   The supplementary data can be found online via the link of http://

810

811

812

Abbreviations

AL–FS   active layer facing feed side
CECP   cake-enhanced concentration polarisation
CEOP   cake-enhanced osmotic pressure
CP   concentration polarisation
CTA   cellulose triacetate
DCP   dilutive concentration polarisation
DI   de-ionised
DS   draw solution
ECP   external concentration polarisation
FO   forward osmosis
FS   feed solution
ICP   internal concentration polarisation
NF   nanofiltration
ODMPs   osmotically driven membrane processes
ORF   osmotic-resistance filtration
RO   reverse osmosis
RSD   reverse solute diffusion

Nomenclature

A water permeability coefficient (m^3/m^2-Pa)
B solute permeability coefficient (m^3/m^2)
C concentration (moles/m^3)
D diffusion coefficient (m^2/s)
F_{cecp} concentration polarization factor for CECP (dimensionless)
F_{dcp} concentration polarization factor for DCP (dimensionless)
F_{ecp} concentration polarization factor for ECP (dimensionless)
J_s solute flux (m^3/m^2 s)
J_w water flux (m^3/m^2 s)
$J_{w,f}$ fouling water flux (m^3/m^2 s)
k mass transfer coefficient (m/s)
k_{cecp} mass transfer coefficient near the membrane surface (m/s)
$k_{ecp,f}$ overall mass transfer coefficient across the foulant layer and external concentration polarization boundary layer (m/s)
$k_{ecp,f}^{*}$ mass transfer coefficient within the foulant layer on the membrane (m/s)
$k_{ecp,o}$ mass transfer coefficient to the ECP boundary layer above the foulant layer (m/s)
M molar (moles/m^3)
m_f mass deposition density (g/m^2)
R_f foulant resistance (m^{-1})
R_f/m_f specific foulant resistance (m/g)
R_g universal gas constant (8.3145 m^3 Pa mol^{-1} K^{-1})
R_m hydraulic resistance of the membrane (m^{-1})
S structural parameter (m^{-1})

860	S_f	structural parameter of the foulant layer (m^{-1})
861	$\overline{S}_f$	overall effective thickness of the CP boundary layer (m)
862	T	temperature (K)
863	TMP	transmembrane pressure (Pa)
864	TOC	total organic carbon (g/m^3)
865	β	van't Hoff coefficient
866	δ	boundary layer thickness (m)
867	μ	fluid viscosity (Pa s)
868	η_{rej}	solute rejection
869	π_{ds}	osmotic pressure of the draw solution (Pa)
870	π_{fs}	osmotic pressure of the feed solution (Pa)
871	$\pi_{fs,m}$	osmotic pressure of the feed solution at the membrane surface (Pa)
872 873	π_i	osmotic pressure of the draw at the interface between the active layer of the membrane and the support
874	$\Delta\pi$	osmotic pressure difference across the membrane (Pa)
875	ΔP	effective applied hydraulic pressure (Pa)
876		
877		

878 **References**

879 [1] T.Y. Cath, A.E. Childress, M. Elimelech, Forward osmosis: Principles, applications, and
880 recent developments, J. Membr. Sci., 281 (2006) 70-87.
881 [2] S. Zhao, L. Zou, C.Y. Tang, D. Mulcahy, Recent developments in forward osmosis:
882 Opportunities and challenges, J. Membr. Sci., 396 (2012) 1-21.
883 [3] R. Valladares Linares, Z. Li, S. Sarp, S. Bucs, G. Amy, J.S. Vrouwenvelder, Forward
884 osmosis niches in seawater desalination and wastewater reuse, Water Res., 66 (2014) 122-139.
885 [4] G. Blandin, A. Verliefde, J. Comas, I. Rodriguez-Roda, P. Le-Clech, Efficiently Combining
886 Water Reuse and Desalination through Forward Osmosis—Reverse Osmosis (FO-RO) Hybrids:
887 A Critical Review, Membranes, 6 (2016) 37.
888 [5] K. Lutchmiah, A.R.D. Verliefde, K. Roest, L.C. Rietveld, E.R. Cornelissen, Forward
889 osmosis for application in wastewater treatment: A review, Water Res., 58 (2014) 179-197.
890 [6] X. Wang, V.W.C. Chang, C.Y. Tang, Osmotic membrane bioreactor (OMBR) technology
891 for wastewater treatment and reclamation: Advances, challenges, and prospects for the future,
892 J. Membr. Sci., 504 (2016) 113-132.
893 [7] B.D. Coday, B.G.M. Yaffe, P. Xu, T.Y. Cath, Rejection of Trace Organic Compounds by
894 Forward Osmosis Membranes: A Literature Review, Environmental Science & Technology,
895 48 (2014) 3612-3624.
896 [8] X. Wang, J. Zhang, V.W.C. Chang, Q. She, C.Y. Tang, Removal of cytostatic drugs from
897 wastewater by an anaerobic osmotic membrane bioreactor, Chem. Eng. J., 339 (2018) 153-161.
898 [9] X. Jin, Q. She, X. Ang, C.Y. Tang, Removal of boron and arsenic by forward osmosis
899 membrane: Influence of membrane orientation and organic fouling, J. Membr. Sci., 389 (2012)
900 182-187.
901 [10] J. Zhang, Q. She, V.W.C. Chang, C.Y. Tang, R.D. Webster, Mining Nutrients (N, K, P)
902 from Urban Source-Separated Urine by Forward Osmosis Dewatering, Environ. Sci. Technol.,
903 48 (2014) 3386-3394.
904 [11] A.J. Ansari, F.I. Hai, W.E. Price, J.E. Drewes, L.D. Nghiem, Forward osmosis as a
905 platform for resource recovery from municipal wastewater - A critical assessment of the
906 literature, J. Membr. Sci., 529 (2017) 195-206.
907 [12] S. Phuntsho, H.K. Shon, S. Hong, S. Lee, S. Vigneswaran, A novel low energy fertilizer
908 driven forward osmosis desalination for direct fertigation: Evaluating the performance of
909 fertilizer draw solutions, J. Membr. Sci., 375 (2011) 172-181.
910 [13] D.L. Shaffer, J.R. Werber, H. Jaramillo, S. Lin, M. Elimelech, Forward osmosis: Where
911 are we now?, Desalination, 356 (2015) 271-284.
912 [14] L. Chekli, S. Phuntsho, J.E. Kim, J. Kim, J.Y. Choi, J.-S. Choi, S. Kim, J.H. Kim, S. Hong,
913 J. Sohn, H.K. Shon, A comprehensive review of hybrid forward osmosis systems: Performance,
914 applications and future prospects, J. Membr. Sci., 497 (2016) 430-449.
915 [15] R.K. McGovern, J.H. Lienhard V, On the potential of forward osmosis to energetically
916 outperform reverse osmosis desalination, J. Membr. Sci., 469 (2014) 245-250.
917 [16] N.M. Mazlan, D. Peshev, A.G. Livingston, Energy consumption for desalination — A
918 comparison of forward osmosis with reverse osmosis, and the potential for perfect membranes,
919 Desalination, 377 (2016) 138-151.
920 [17] T.-S. Chung, L. Luo, C.F. Wan, Y. Cui, G. Amy, What is next for forward osmosis (FO)
921 and pressure retarded osmosis (PRO), Sep. Purif. Technol., 156 (2015) 856-860.
922 [18] A. Achilli, T.Y. Cath, E.A. Marchand, A.E. Childress, The forward osmosis membrane
923 bioreactor: A low fouling alternative to MBR processes, Desalination, 238 (2009) 10-21.
924 [19] B. Mi, M. Elimelech, Organic fouling of forward osmosis membranes: Fouling
925 reversibility and cleaning without chemical reagents, J. Membr. Sci., 348 (2010) 337-345.

926 [20] S. Lee, C. Boo, M. Elimelech, S. Hong, Comparison of fouling behavior in forward
927 osmosis (FO) and reverse osmosis (RO), J. Membr. Sci., 365 (2010) 34-39.
928 [21] B. Mi, M. Elimelech, Silica scaling and scaling reversibility in forward osmosis,
929 Desalination, 312 (2013) 75-81.
930 [22] Y. Kim, M. Elimelech, H.K. Shon, S. Hong, Combined organic and colloidal fouling in
931 forward osmosis: Fouling reversibility and the role of applied pressure, J. Membr. Sci., 460
932 (2014) 206-212.
933 [23] S.E. Kwan, E. Bar-Zeev, M. Elimelech, Biofouling in forward osmosis and reverse
934 osmosis: Measurements and mechanisms, J. Membr. Sci., 493 (2015) 703-708.
935 [24] M. Xie, J. Lee, L.D. Nghiem, M. Elimelech, Role of pressure in organic fouling in forward
936 osmosis and reverse osmosis, J. Membr. Sci., 493 (2015) 748-754.
937 [25] F. Lotfi, L. Chekli, S. Phuntsho, S. Hong, J.Y. Choi, H.K. Shon, Understanding the
938 possible underlying mechanisms for low fouling tendency of the forward osmosis and pressure
939 assisted osmosis processes, Desalination, (2017).
940 [26] Y. Yu, S. Lee, S.K. Maeng, Forward osmosis membrane fouling and cleaning for
941 wastewater reuse, Journal of Water Reuse and Desalination, 7 (2017) 111-120.
942 [27] J. Lee, S. Kook, C. Lee, I.S. Kim, Effect of intermittent pressure-assisted forward osmosis
943 (I-PAFO) on organic fouling, Desalination, 419 (2017) 60-69.
944 [28] G. Blandin, A.R.D. Verliefde, P. Le-Clech, Pressure enhanced fouling and adapted anti-
945 fouling strategy in pressure assisted osmosis (PAO), J. Membr. Sci., 493 (2015) 557-567.
946 [29] W.C.L. Lay, T.H. Chong, C.Y. Tang, A.G. Fane, J. Zhang, Y. Liu, Fouling propensity of
947 forward osmosis: Investigation of the slower flux decline phenomenon, Water Sci. Technol.,
948 61 (2010) 927-936.
949 [30] Y. Jang, H. Cho, Y. Shin, Y. Choi, S. Lee, J. Koo, Comparison of fouling propensity and
950 physical cleaning effect in forward osmosis, reverse osmosis, and membrane distillation,
951 Desalination and Water Treatment, 57 (2016) 24532-24541.
952 [31] E.W. Tow, J.H. Lienhard V, Quantifying osmotic membrane fouling to enable
953 comparisons across diverse processes, J. Membr. Sci., 511 (2016) 92-107.
954 [32] A.G. Fane, T.H. Chong, J. Zhang, W.C.L. Lay, The Effect of Flux and Pressure on Fouling
955 in Reverse Osmosis Desalination, Proceedings IDA World Congress, (2009) Paper DB09-128.
956 [33] R.W. Field, G.K. Pearce, Critical, sustainable and threshold fluxes for membrane filtration
957 with water industry applications, Adv. Colloid Interface Sci., 164 (2011) 38-44.
958 [34] Z. Xie, N. Nagaraja, L. Skillman, D. Li, G. Ho, Comparison of polysaccharide fouling in
959 forward osmosis and reverse osmosis separations, Desalination, 402 (2017) 174-184.
960 [35] J.R. McCutcheon, M. Elimelech, Influence of concentrative and dilutive internal
961 concentration polarization on flux behavior in forward osmosis, J. Membr. Sci., 284 (2006)
962 237-247.
963 [36] C.Y. Tang, Q. She, W.C.L. Lay, R. Wang, A.G. Fane, Coupled effects of internal
964 concentration polarization and fouling on flux behavior of forward osmosis membranes during
965 humic acid filtration, J. Membr. Sci., 354 (2010) 123-133.
966 [37] Q. She, R. Wang, A.G. Fane, C.Y. Tang, Membrane fouling in osmotically driven
967 membrane processes: A review, J. Membr. Sci., 499 (2016) 201-233.
968 [38] E.M.V. Hoek, M. Elimelech, Cake-Enhanced Concentration Polarization: A New Fouling
969 Mechanism for Salt-Rejecting Membranes, Environ. Sci. Technol., 37 (2003) 5581-5588.
970 [39] T.H. Chong, F.S. Wong, A.G. Fane, Implications of critical flux and cake enhanced
971 osmotic pressure (CEOP) on colloidal fouling in reverse osmosis: Experimental observations,
972 J. Membr. Sci., 314 (2008) 101-111.
973 [40] C.Y. Tang, Y.N. Kwon, J.O. Leckie, Characterization of humic acid fouled reverse
974 osmosis and nanofiltration membranes by transmission electron microscopy and streaming
975 potential measurements, Environ. Sci. Technol., 41 (2007) 942-949.

976 [41] A. Tiraferri, N.Y. Yip, A.P. Straub, S. Romero-Vargas Castrillon, M. Elimelech, A method
977 for the simultaneous determination of transport and structural parameters of forward osmosis
978 membranes, J. Membr. Sci., 444 (2013) 523-538.
979 [42] A.J. Karabelas, D.C. Sioutopoulos, Toward improvement of methods for predicting
980 fouling of desalination membranes — The effect of permeate flux on specific fouling resistance,
981 Desalination, 343 (2014) 97-105.
982 [43] Q. She, Y.K.W. Wong, S. Zhao, C.Y. Tang, Organic fouling in pressure retarded osmosis:
983 Experiments, mechanisms and implications, J. Membr. Sci., 428 (2013) 181-189.
984 [44] Q. She, X. Jin, Q. Li, C.Y. Tang, Relating reverse and forward solute diffusion to
985 membrane fouling in osmotically driven membrane processes, Water Res., 46 (2012) 2478-
986 2486.
987 [45] Q. She, D. Hou, J. Liu, K.H. Tan, C.Y. Tang, Effect of feed spacer induced membrane
988 deformation on the performance of pressure retarded osmosis (PRO): Implications for PRO
989 process operation, J. Membr. Sci., 445 (2013) 170-182.
990 [46] E.M.V. Hoek, A.S. Kim, M. Elimelech, Influence of crossflow membrane filter geometry
991 and shear rate on colloidal fouling in reverse osmosis and nanofiltration separations,
992 Environmental Engineering Science, 19 (2002) 357-372.
993 [47] C.Y. Tang, T.H. Chong, A.G. Fane, Colloidal interactions and fouling of NF and RO
994 membranes: A review, Adv. Colloid Interface Sci., 164 (2011) 126-143.
995 [48] R.W. Field, J.J. Wu, Mass transfer limitations in forward osmosis: Are some potential
996 applications overhyped?, Desalination, 318 (2013) 118-124.
997 [49] T.Y. Cath, M. Elimelech, J.R. McCutcheon, R.L. McGinnis, A. Achilli, D. Anastasio, A.R.
998 Brady, A.E. Childress, I.V. Farr, N.T. Hancock, J. Lampi, L.D. Nghiem, M. Xie, N.Y. Yip,
999 Standard Methodology for Evaluating Membrane Performance in Osmotically Driven
1000 Membrane Processes, Desalination, (2012).
1001 [50] B. Kim, G. Gwak, S. Hong, Review on methodology for determining forward osmosis
1002 (FO) membrane characteristics: Water permeability (A), solute permeability (B), and structural
1003 parameter (S), Desalination, 422 (2017) 5-16.
1004 [51] B. Mi, M. Elimelech, Gypsum scaling and cleaning in forward osmosis: Measurements
1005 and mechanisms, Environ. Sci. Technol., 44 (2010) 2022-2028.
1006 [52] L. Song, M. Elimelech, Particle Deposition onto a Permeable Surface in Laminar Flow, J.
1007 Colloid Interface Sci., 173 (1995) 165-180.
1008 [53] L.N. Sim, Y. Ye, V. Chen, A.G. Fane, Investigations of the coupled effect of cake-
1009 enhanced osmotic pressure and colloidal fouling in RO using crossflow sampler-modified
1010 fouling index ultrafiltration, Desalination, 273 (2011) 184-196.
1011 [54] C.Y. Tang, J.O. Leckie, Membrane independent limiting flux for RO and NF membranes
1012 fouled by humic acid, Environ. Sci. Technol., 41 (2007) 4767-4773.
1013 [55] E.W. Tow, J.H. Lienhard V, Unpacking compaction: Effect of hydraulic pressure on
1014 alginate fouling, J. Membr. Sci., 544 (2017) 221-233.
1015 [56] A. Rushton, A.S. Ward, R.G. Holdich, Solid-Liquid Filtration and Separation Technology,
1016 Wiley-VCH, 1996.
1017 [57] R. Guha, X. Shang, A.L. Zydney, D. Velegol, M. Kumar, Diffusiophoresis contributes
1018 significantly to colloidal fouling in low salinity reverse osmosis systems, J. Membr. Sci., 479
1019 (2015) 67-76.
1020 [58] M. Zhang, D. Hou, Q. She, C.Y. Tang, Gypsum scaling in pressure retarded osmosis:
1021 Experiments, mechanisms and implications, Water Res., 48 (2014) 387-395.
1022 [59] M. Zhang, Q. She, X. Yan, C.Y. Tang, Effect of reverse solute diffusion on scaling in
1023 forward osmosis: A new control strategy by tailoring draw solution chemistry, Desalination,
1024 401 (2017) 230-237.

1025   [60] P. van den Brink, A. Zwijnenburg, G. Smith, H. Temmink, M. van Loosdrecht, Effect of
1026   free calcium concentration and ionic strength on alginate fouling in cross-flow membrane
1027   filtration, J. Membr. Sci., 345 (2009) 207-216.
1028   [61] S. Meng, Y. Liu, Transparent exopolymer particles (TEP)-associated membrane fouling
1029   at different Na+ concentrations, Water Res., 111 (2017) 52-58.
1030   [62] J. BAUMY, J., G. BRULE, Effect of pH and ionic strength on the binding of bivalent
1031   cations to β-casein, Lait, 68 (1988) 409-417.
1032   [63] K.J. Thomas, C.V. Rice, Revised model of calcium and magnesium binding to the
1033   bacterial cell wall, BioMetals, 27 (2014) 1361-1370.
1034   [64] R.W. Field, J.J. Wu, Modelling of permeability loss in membrane filtration: Re-
1035   examination of fundamental fouling equations and their link to critical flux, Desalination, 283
1036   (2011) 68-74.
1037